Deep-Learning-Based Cosmic-Ray Mass Reconstruction Using the Water-Cherenkov and Scintillation Detectors of AugerPrime

Niklas Langner[a,*] **for the Pierre Auger Collaboration**[b]

[a]*RWTH Aachen University, III. Physikalisches Institut A,*
Aachen, Germany

[b]*Observatorio Pierre Auger, Av. San Martín Norte 304, 5613 Malargüe, Argentina*
Full author list: https://www.auger.org/archive/authors_icrc_2023.html

E-mail: spokespersons@auger.org

At the highest energies, cosmic rays can be detected only indirectly by the extensive air showers they create upon interaction with the Earth's atmosphere. While high-statistics measurements of the energy and arrival directions of cosmic rays can be performed with large surface detector arrays like the Pierre Auger Observatory, the determination of the cosmic-ray mass on an event-by-event basis is challenging. Meaningful physical observables in this regard include the depth of maximum of air-shower profiles, which is related to the mean free path of the cosmic ray in the atmosphere and the shower development, as well as the number of muons that rises with the number of nucleons in a cosmic-ray particle.

In this contribution, we present an approach to determine both of these observables from combined measurements of water-Cherenkov detectors and scintillation detectors, which are part of the AugerPrime upgrade of the Observatory. To characterize the time-dependent signals of the two detectors both separately as well as in correlation to each other, we apply deep learning techniques. Transformer networks employing the attention mechanism are especially well-suited for this task. We present the utilized network concepts and apply them to simulations to determine the precision of the event-by-event mass reconstruction that can be achieved by the combined measurements of the depth of shower maximum and the number of muons.

---

*Speaker

1. Introduction

An event-by-event measurement of the masses of ultra-high-energy cosmic rays poses the potential to enable new insights regarding their sources. Observables related to the cosmic-ray mass include the atmospheric depth of shower maximum $X_{\max}$ which relates to the mean free path of the cosmic ray in the atmosphere and the shower development, as well as the number of muons R_μ that rises with the number of nucleons in the primary particle. At the Pierre Auger Observatory [1], $X_{\max}$ can be obtained with the Fluorescence Detector [2] which operates at moonless nights. Recently, deep learning approaches have been utilized to reconstruct $X_{\max}$ from measurements of the Surface Detector array (SD) [3], providing significantly increased statistics due to its duty cycle of close to 100% [4, 5]. The same approach can be used to reconstruct R_μ [6]. Currently, the Pierre Auger Observatory is undergoing an enhancement in form of the AugerPrime upgrade which will further increase the mass sensitivity of the SD. In particular, equipping the water-Cherenkov detectors (WCDs) of the SD with additional scintillators (SSDs) [7] will allow for a better separation of electromagnetic and muonic shower components [8–10].

In this contribution, we present an extension of the deep learning approach to reconstruct R_μ in addition to $X_{\max}$ on an event-by-event basis with a single neural network. We show how a Transformer-based deep neural network (DNN) can be applied to process the joint measurements of WCD and SSD traces. The DNN is trained and evaluated using simulations to estimate the improvement in mass sensitivity by the AugerPrime upgrade. Finally, introspection methods are applied to assess the individual importance of the WCDs and SSDs for the predictions of the DNN.

2. The AugerPrime Surface Detector

As part of the AugerPrime upgrade [8–10], each station of the SD is being equipped with multiple new components that both enhance and complement the WCDs. While the dynamic range of the WCDs is extended with the addition of a fourth photomultiplier (PMT) with a significantly smaller cathode surface, an additional radio antenna [11] and scintillation detector [7] provide new capabilities in the measurement of air showers. SSD modules are mounted on top of the WCDs and consist of two scintillator elements covering an area of 1.9 m^2 each. With the SSD being especially sensitive to the electromagnetic shower component and the WCD measuring both the muonic and the electromagnetic components, a better separation between the two shower components can be achieved by combining the two measurements [8–10]. In addition, the Unified Board (UB) used for readout of the detectors is replaced by the Upgraded Unified Board [12] (UUB), resulting in a threefold increase of the readout frequency from 40 MHz to 120 MHz. In this work, the impact of the UUB and SSD on the cosmic-ray mass sensitivity with a Transformer-based DNN will be examined. The DNN is applied to the time traces recorded by the three large PMTs of the WCD and the PMT of the SSD. For WCD measurements with UB, a three-dimensional time trace with 120 time steps of 25 ns is used per station. The tracelength increases to 360 time steps of 8.3 ns when using the UUB.
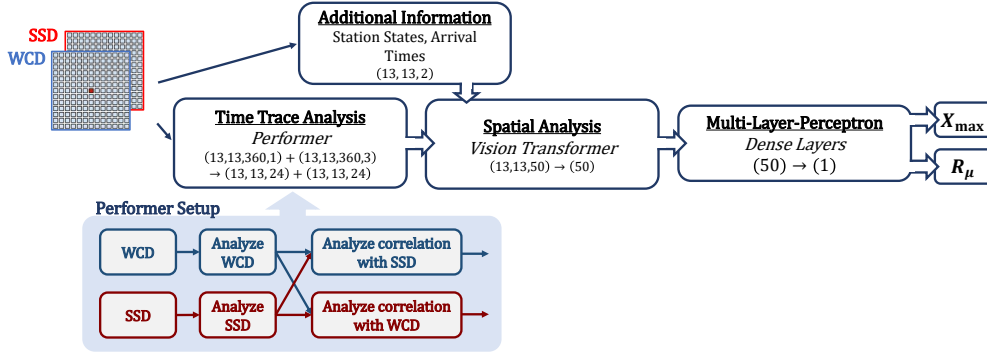
Figure 1: Full architecture of the Transformer-based neural network. The Performer setup performs both self-attention of the individual detectors as well as a cross-attention to analyze their correlations.

3. Transformer-Based Neural Network

To extract information regarding the primary cosmic-ray mass from the highly complex measurements of the AugerPrime SD, a deep-learning approach is applied. The DNN consists of two parts which analyse the time traces on station-level and the whole shower footprint on a grid-level, respectively. A similar approach previously utilized recurrent networks (RNNs) in conjunction with convolutional networks (CNNs) to determine the depth of shower maximum X_{max} from WCD time traces [4, 5]. Here, the RNNs and CNNs are replaced by attention-based Transformers [13] and R_μ, the number of muons with removed energy- and zenith-dependence as seen on simulations, is introduced as an additional output of the DNN. In particular, an efficient Performer [14] is used to perform the time trace analysis, while the hexagonal grid that constitutes the shower footprint is processed by a Vision Transformer typically used for image recognition [15].

Preprocessing The DNN is provided with the inputs for each station: three WCD traces, one SSD trace, first particle arrival times and station states. The preprocessing is based on [4] with some adjustments due to the additional SSD traces and the higher sampling frequency of the UUB: A subgrid of 13×13 SD stations centered around the station with the largest signal is used to reduce memory requirements while keeping most of the signal. Given that large numerical fluctuations might hinder the training process of the DNN, both WCD and SSD time traces $S_i(t)$ are transformed with a logarithmic re-scaling following $\tilde{S}(t) = \log_{10}(S_i(t)/\mathrm{VEM} + 1)$. To normalize the time traces, both WCD and SSD are divided by their respective standard deviation of $\tilde{S}$ in the training data. The particle arrival times are given relative to the central station and also normalized in the same way. While the DNN is trained on simulations, a clipping at high signal values simulates the saturation of real measurements. In addition, a small fraction of individual PMTs and stations are randomly set to zero to simulate non-functioning or non-existing stations and PMTs. Information regarding whether or not a measurement from a station is present is given to the DNN in form of the station states encoded by ones and zeros.

Time Trace Analysis At the first stage of the DNN, the above-mentioned Performer approach is used for a joint analysis of the WCD and SSD traces on a station-level, reducing the traces to 24

characteristic values each. The attention mechanism of the Performer is capable of processing long sequences of 360 timesteps. In addition, it allows for an individual evaluation of the two trace types (self-attention) as well as their correlation (cross-attention). The self-attention accounts for the different working principles and sensitivities to different shower components of the two detectors while the cross-attention acknowledges their complementary nature when describing the same air shower. DNNs using only WCD traces are trained by performing two consecutive self-attentions.

Spatial Analysis of Shower Footprint For the spatial analysis, the output of the time trace analysis is combined with the information regarding the arrival times and station states, resulting in a vector of 50 values per station. A self-attention over all stations is performed using a Vision Transformer, where the DNN can incorporate geometrical conditions through learnable Embeddings. Afterwards, the total shower is reduced to 50 characteristic values by averaging over all stations.

Network Output Finally, two separate multi-layer-perceptrons transform the 50 values representing the whole air shower to the desired outputs of $X_{\max}$ and R_μ. The full DNN architecture is shown in Fig. 1. During the training process, the simulated true values of $X_{\max}$ and R_μ are used as targets for the network prediction. In an iterative process, the network parameters are adjusted to reduce the loss function, which is given by an element-wise mean squared error in both cases.

4. Performance on Simulations

The DNN is trained using more than $300,000$ simulated air showers with a mixed composition of hydrogen, helium, oxygen and iron, generated with CORSIKA [17] utilizing the EPOS-LHC [18] hadronic interaction model. The test set consists of around $56,000$ simulated showers not used for the training process to allow for an unbiased evaluation of the performance. The energy spectrum of the simulations follows E^{-1} with a range from 3 to 160 EeV ($1\text{EeV} = 10^{18}\text{eV}$). The zenith angle θ ranges from $0°$ to $65°$ and is uniformly distributed in $\cos^2(\theta)$. In Fig. 2, the DNN reconstruction is compared to Monte Carlo (MC) values, where $X_{\max}$ is given as energy-corrected by the elongation rate following $X_{\max} - 56 \cdot \log_{10}(E/\text{EeV})$ to better reflect the mass sensitivity of the DNN. The correlation of $R_{\mu,\text{DNN}}$ with $R_{\mu,\text{MC}}$ increases noticeably from $0.612(3)$ to $0.679(2)$ through the inclusion of the UUB and SSD. The correlation of $X_{\max,\text{DNN}}$ with $X_{\max,\text{MC}}$ increases from $0.861(1)$ to $0.873(1)$. Fig. 2 on the right compares the event-by-event resolution of the network using WCD and SSD with UUB to the network using WCD with UB as a function of the energy reconstructed by the SD. The R_μ profits most notably from the inclusion of SSD and UUB, in particular at high energies. $\sigma(X_{\max})$ is reduced to a lesser extent without a clear energy-dependence. It was found that the improvements of both R_μ and $X_{\max}$ rely mainly on the SSD, while the UUB provides only a small gain in performance. The much more noticeable improvement of R_μ matches the expectation that the combination of WCD and SSD is particularly well-suited to enable a better separation of the electromagnetic and muonic shower components. By combining the two predictions of the DNN into one observable Y, a powerful mass estimator can be obtained. Y is constructed by

$$Y = \hat{R}_\mu - 0.5 \cdot \hat{X}_{\max}, \tag{1}$$

where the hat denotes a normalization $\hat{x} = [x - \text{mean}(x)]/\text{std}(x)$ that ensures that both $\hat{R}_\mu$ and $\hat{X}_{\max}$ cover a similar numerical range. Typical values obtained from simulations are used for the
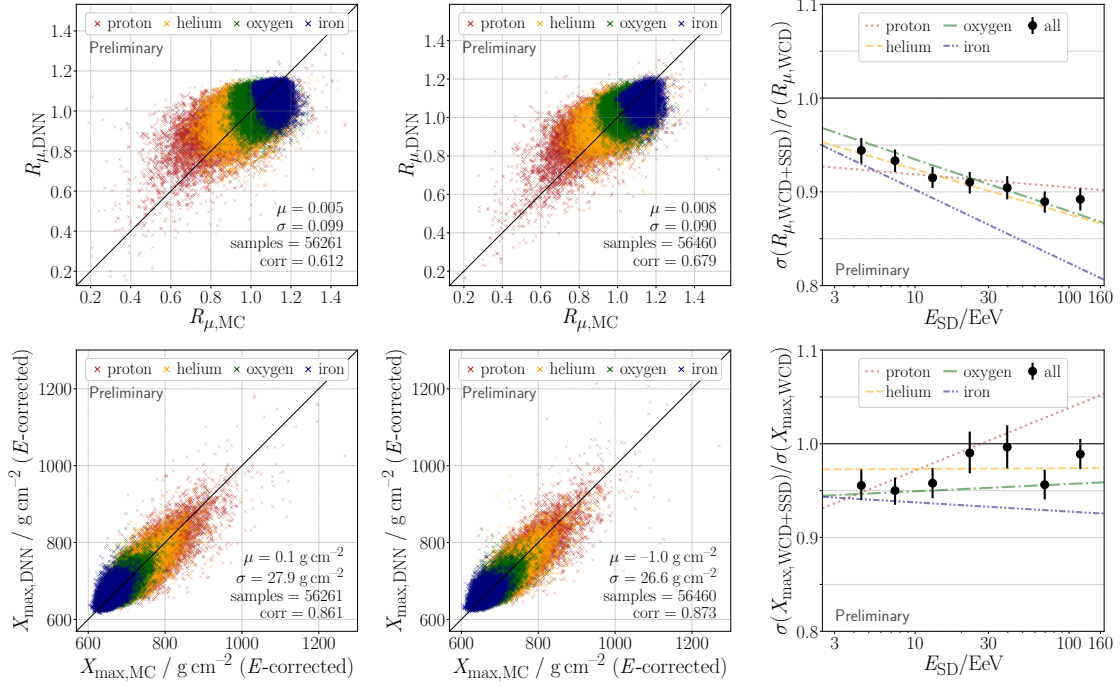
Figure 2: R_μ and X_{max} reconstruction on test dataset not used for training. *(Left)* DNN using WCD time traces with UB. *(Center)* DNN using WCD and SSD time traces with UUB. *(Right)* Improvement in relative resolution when comparing WCD+SSD (UUB) to WCD (UB).
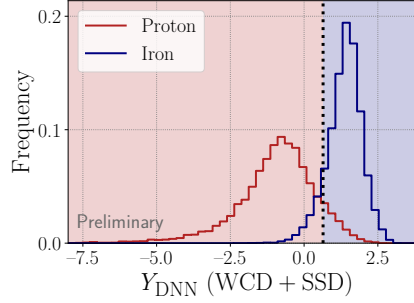

Figure 3: Distribution of Y for proton and iron constructed from DNN outputs. A cut at the dashed line results in a classification accuracy of 90%.

mean and standard deviations to avoid a dependence on the specific test set. The distribution of Y for the proton and iron showers of the test set is shown in Fig. 3. The distributions of Y show strong mass separation with two peaks that feature only a small overlap. Performing a classification via a simple cut on Y as indicated by the dashed line and shaded areas in Fig. 3, 90% (87%) of the proton and iron showers of the test set are correctly classified as such by the WCD+SSD (WCD UB) DNN. The reliable identification of proton-induced air showers is a particularly relevant task when studying the cosmic-ray mass composition. This can be achieved by a high proton identification efficiency with as little misclassified iron showers as possible. To judge the ability of the DNNs, a Y cut is determined that results in a high proton identification efficiency of 80%. The probability of
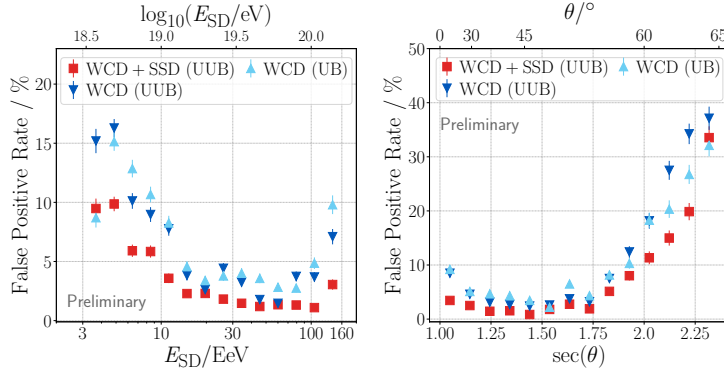
Figure 4: Iron contamination (False Positive Rate) at 80% proton efficiency. *(Left)* As a function of SD-reconstructed energy E_{SD}. *(Right)* As a function of zenith angle θ.
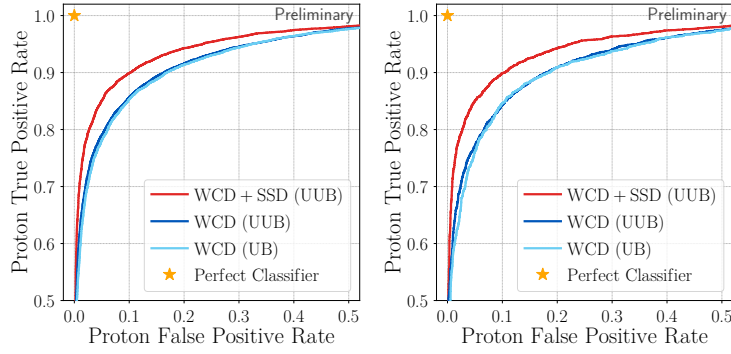

Figure 5: Receiver Operating Characteristic (ROC) curve for proton identification. *(Left)* Zenith range from $0°$ to $65°$. *(Right)* Zenith range from $0°$ to $30°$.

an iron shower being misclassified as a proton shower at this specific cut is shown as a function of energy and zenith angle in Fig. 4. Overall, the iron misclassification is strongly reduced by the UUB and SSD, in particular by the SSD. Over the full energy- and zenith-range, the WCD+SSD DNN exhibits an iron contamination that is either similar or greatly reduced compared to the WCD (UB) DNN, with a typical reduction by a factor of around 2. By varying the cut on Y, different pay-offs regarding the efficiency and purity of the proton classification can be achieved. To evaluate the general classification capability of the DNNs, the True Positive Rate (TPR) and False Positive Rate (FPR) for proton identification are calculated while shifting the cut through the Y-distributions, resulting in Receiver Operating Characteristic (ROC) curves shown in Fig. 5. The WCD+SSD DNN consistently outperforms the DNNs using only the WCD as the red curve is always left of the blue curves. The ROC curves of the two WCD DNNs using the UB or UUB are very close to each other, indicating that the increase in mass separation relies mainly on the SSD. As shown in Fig. 5 on the right, the difference increases when limiting the zenith range to angles up to $30°$, showing that the SSD provides a stronger improvement at low zenith angles, which is expected due to the geometric properties of the detector. Setting the FPR of proton identification to a value of only 1%, the WCD+SSD DNN still achieves a proton TPR of 71%, while the WCD DNNs reach a TPR of
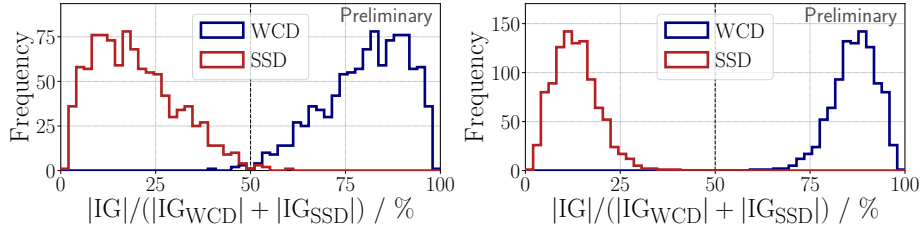
Figure 6: Contribution to the DNN prediction by individual detector components. *(Left)* Integrated Gradients (IG) fraction for R_μ prediction. *(Right)* IG fraction for X_{max} prediction.
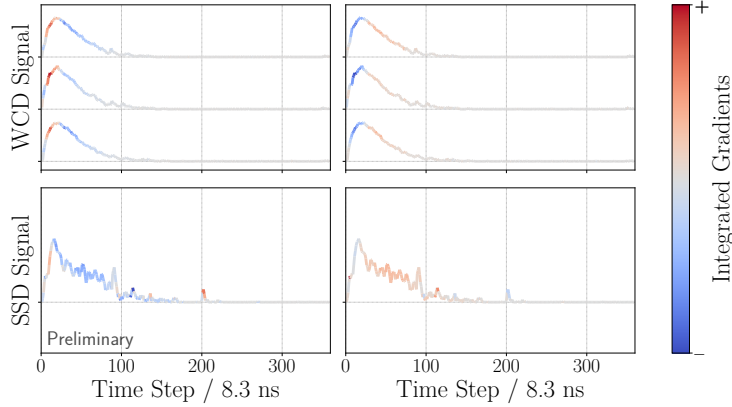

Figure 7: Contribution to the DNN prediction by individual parts of the time traces of the central station. *(Left)* Influence on R_μ prediction. *(Right)* Influence on X_{max} prediction.

61% with the UUB and 58% with the UB, once again showing the strong impact of the SSD.

5. Importance of Individual Detectors

While the inclusion of the SSD leads to an improved mass separation power of the DNN, it is still to be investigated how the DNN uses the additional input and to what degree the individual detectors influence the final predictions of R_μ and X_{max}. This question is answered by applying Integrated Gradients [19] (IG) to the DNN, an attribution method that provides individual importance values for input features with respect to a specific output. By comparing the IG values for the WCD and SSD traces to the total sum of IG for both sets of time traces, a relative importance of the two detectors can be obtained. The distribution of the importance of both detectors is shown in Fig. 6, calculated from 1000 showers of the test set. For both R_μ (Fig. 6 Left) and X_{max} (Fig. 6 right), the WCD is the most important of the two detectors, with a mean importance of 80% and 87%, respectively. Once again, the R_μ reconstruction is found to profit more strongly from the SSD, sometimes even relying more on the SSD than on the WCD. Limiting the zenith range to angles up to 30°, the importance of the SSD increases to 23% (15%) for the reconstruction of R_μ (X_{max}), confirming the zenith-dependence of SSD usage observed in Fig. 5. In addition to the IG sum of the traces, the individual contribution of each timestep can be analysed. The influence of the traces of the central station on the DNN reconstruction are shown for both outputs in Fig. 7. The opposite influence of the parts of the traces when comparing R_μ (Fig. 7 left) and X_{max} (Fig. 7 right) matches

the expectation that the two observables are anti-correlated. The different influences of the rising and falling edges also match the expectation of the rising edge being dominated by muons, while late muon peaks are observed to have a strong positive impact on R_μ.

6. Conclusion

The new components added to the surface detector stations of the Pierre Auger Observatory as part of the AugerPrime upgrade necessitate novel approaches to effectively analyse the highly complex measurements. A Transformer-based network is able to handle the increased trace length by the UUB, and in addition provides an efficient way to analyse the joint measurement of WCD and SSD. The network presented here processes the time traces on station-level using a Performer, followed by a Vision Transformer that analyses the whole shower footprint on a hexagonal grid. It was found on simulations that the additional measurements provided by the SSD improve both the X_{max} and R_μ reconstruction, with a particular strong benefit for the R_μ reconstruction. By combining both observables to obtain a single mass estimator Y, a reasonable mass separation between proton and iron can be achieved, where the inclusion of the SSD strongly reduces the misclassification of iron. The performance gain by the SSD is particularly pronounced at lower zenith angles and attribution methods show that the DNN bases its prediction on the SSD with an importance of around 20%, while the importance of the WCD is found to be roughly 80%. The influence of individual parts of the time traces matches physics expectations, indicating the capability of the Transformer-based network to process the joint measurement in a meaningful way. In the future, developments like directly encoding arrival times in the time traces or using a large standard Transformer instead of the Performer as more resources become available are expected to further increase the performance.

References

[1] A. Aab *et al.* [Pierre Auger coll.], Nucl. Instrum. Meth. A **798** (2015) 172-213.

[2] A. Aab *et al.* [Pierre Auger coll.], Phys. Rev. D **90**, (2014) 122005.

[3] I. Allekotte *et al.*, Nucl. Instrum. Meth. A **586** (2008) 409-420.

[4] A. Aab *et al.* [Pierre Auger coll.], JINST **16** (2021) P07019.

[5] J. Glombitza *et al.* [Pierre Auger coll.], PoS **ICRC2023** (2023) 278.

[6] S. Hahn *et al.* [Pierre Auger coll.], PoS **ICRC2023** (2023) 318.

[7] R. Šmída *et al.* [Pierre Auger coll.], PoS **ICRC2017** (2017) 390.

[8] A. Aab *et al.* [Pierre Auger coll.], arXiv preprint arXiv:1604.03637 (2016).

[9] D. Martello *et al.* [Pierre Auger coll.], PoS **ICRC2017** (2017) 383.

[10] A. Castellina *et al.* [Pierre Auger coll.], EPJ Web of Conferences **210**, (2019) 06002.

[11] T. Huege *et al.* [Pierre Auger coll.], EPJ Web Conf. **283** (2023) 06002.

[12] D. Nitz *et al.* [Pierre Auger coll.], PoS **ICRC2019** (2019) 370.

[13] A. Vaswani *et al.*, Advances In Neural Information Processing Systems **30** (2017).

[14] K. Choromanski *et al.*, International Conference on Learning Representations (2021).

[15] A. Dosovitskiy *et al.*, International Conference on Learning Representations (2021).

[16] D. Hendrycks and K. Gimpel, International Conference on Learning Representations (2017).

[17] D. Heck *et al.*, Forschungszentrum Karlsruhe Report FZKA **6019** (1998).

[18] T. Pierog *et al.*, Physik. Rev. C **92**, (2015) 034906.

[19] M. Sundararajan *et al.*, Proceedings of the 34th International Conference on Machine Learning, PMLR **70** (2017) 3319-3328.

The Pierre Auger Collaboration
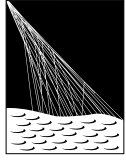
PIERRE AUGER OBSERVATORY

A. Abdul Halim[13], P. Abreu[72], M. Aglietta[54,52], I. Allekotte[1], K. Almeida Cheminant[70], A. Almela[7,12], R. Aloisio[45,46], J. Alvarez-Muñiz[79], J. Ammerman Yebra[79], G.A. Anastasi[54,52], L. Anchordoqui[86], B. Andrada[7], S. Andringa[72], C. Aramo[50], P.R. Araújo Ferreira[42], E. Arnone[63,52], J. C. Arteaga Velázquez[67], H. Asorey[7], P. Assis[72], G. Avila[11], E. Avocone[57,46], A.M. Badescu[75], A. Bakalova[32], A. Balaceanu[73], F. Barbato[45,46], A. Bartz Mocellin[85], J.A. Bellido[13,69], C. Berat[36], M.E. Bertaina[63,52], G. Bhatta[70], M. Bianciotto[63,52], P.L. Biermann[h], V. Binet[5], K. Bismark[39,7], T. Bister[80,81], J. Biteau[37], J. Blazek[32], C. Bleve[36], J. Blümer[41], M. Boháčová[32], D. Boncioli[57,46], C. Bonifazi[8,26], L. Bonneau Arbeletche[21], N. Borodai[70], J. Brack[j], P.G. Brichetto Orchera[7], F.L. Briechle[42], A. Bueno[78], S. Buitink[15], M. Buscemi[47,61], M. Büsken[39,7], A. Bwembya[80,81], K.S. Caballero-Mora[66], S. Cabana-Freire[79], L. Caccianiga[59,49], I. Caracas[38], R. Caruso[58,47], A. Castellina[54,52], F. Catalani[18], G. Cataldi[48], L. Cazon[79], M. Cerda[10], A. Cermenati[45,46], J.A. Chinellato[21], J. Chudoba[32], L. Chytka[33], R.W. Clay[13], A.C. Cobos Cerutti[6], R. Colalillo[60,50], A. Coleman[90], M.R. Coluccia[48], R. Conceição[72], A. Condorelli[37], G. Consolati[49,55], M. Conte[56,48], F. Convenga[41], D. Correia dos Santos[28], P.J. Costa[72], C.E. Covault[84], M. Cristinziani[44], C.S. Cruz Sanchez[3], S. Dasso[4,2], K. Daumiller[41], B.R. Dawson[13], R.M. de Almeida[28], J. de Jesús[7,41], S.J. de Jong[80,81], J.R.T. de Mello Neto[26,27], I. De Mitri[45,46], J. de Oliveira[17], D. de Oliveira Franco[21], F. de Palma[56,48], V. de Souza[19], E. De Vito[56,48], A. Del Popolo[58,47], O. Deligny[34], N. Denner[32], L. Deval[41,7], A. di Matteo[52], M. Dobre[73], C. Dobrigkeit[21], J.C. D'Olivo[68], L.M. Domingues Mendes[72], J.C. dos Anjos, R.C. dos Anjos[25], J. Ebr[32], F. Ellwanger[41], M. Emam[80,81], R. Engel[39,41], I. Epicoco[56,48], M. Erdmann[42], A. Etchegoyen[7,12], C. Evoli[45,46], H. Falcke[80,82,81], J. Farmer[89], G. Farrar[88], A.C. Fauth[21], N. Fazzini[e], F. Feldbusch[40], F. Fenu[41,d], A. Fernandes[72], B. Fick[87], J.M. Figueira[7], A. Filipčič[77,76], T. Fitoussi[41], B. Flaggs[90], T. Fodran[80], T. Fujii[89,f], A. Fuster[7,12], C. Galea[80], C. Galelli[59,49], B. García[6], C. Gaudu[38], H. Gemmeke[40], F. Gesualdi[7,41], A. Gherghel-Lascu[73], P.L. Ghia[34], U. Giaccari[48], M. Giammarchi[49], J. Glombitza[42,g], F. Gobbi[10], F. Gollan[7], G. Golup[1], M. Gómez Berisso[1], P.F. Gómez Vitale[11], J.P. Gongora[11], J.M. González[1], N. González[7], I. Goos[1], D. Góra[70], A. Gorgi[54,52], M. Gottowik[79], T.D. Grubb[13], F. Guarino[60,50], G.P. Guedes[22], E. Guido[44], S. Hahn[39], P. Hamal[32], M.R. Hampel[7], P. Hansen[3], D. Harari[1], V.M. Harvey[13], A. Haungs[41], T. Hebbeker[42], C. Hojvat[e], J.R. Hörandel[80,81], P. Horvath[33], M. Hrabovský[33], T. Huege[41,15], A. Insolia[58,47], P.G. Isar[74], P. Janecek[32], J.A. Johnsen[85], J. Jurysek[32], A. Kääpä[38], K.H. Kampert[38], B. Keilhauer[41], A. Khakurdikar[80], V.V. Kizakke Covilakam[7,41], H.O. Klages[41], M. Kleifges[40], F. Knapp[39], N. Kunka[40], B.L. Lago[16], N. Langner[42], M.A. Leigui de Oliveira[24], Y Lema-Capeans[79], V. Lenok[39], A. Letessier-Selvon[35], I. Lhenry-Yvon[34], D. Lo Presti[58,47], L. Lopes[72], L. Lu[91], Q. Luce[39], J.P. Lundquist[76], A. Machado Payeras[21], M. Majercakova[32], D. Mandat[32], B.C. Manning[13], P. Mantsch[e], S. Marafico[34], F.M. Mariani[59,49], A.G. Mariazzi[3], I.C. Mariş[14], G. Marsella[61,47], D. Martello[56,48], S. Martinelli[41,7], O. Martínez Bravo[64], M.A. Martins[79], M. Mastrodicasa[57,46], H.J. Mathes[41], J. Matthews[a], G. Matthiae[62,51], E. Mayotte[85,38], S. Mayotte[85], P.O. Mazur[e], G. Medina-Tanco[68], J. Meinert[38], D. Melo[7], A. Menshikov[40], C. Merx[41], S. Michal[33], M.I. Micheletti[5], L. Miramonti[59,49], S. Mollerach[1], F. Montanet[36], L. Morejon[38], C. Morello[54,52], A.L. Müller[32], K. Mulrey[80,81], R. Mussa[52], M. Muzio[88], W.M. Namasaka[38], S. Negi[32], L. Nellen[68], K. Nguyen[87], G. Nicora[9], M. Niculescu-Oglinzanu[73], M. Niechciol[44], D. Nitz[87], D. Nosek[31], V. Novotny[31], L. Nožka[33], A Nucita[56,48], L.A. Núñez[30], C. Oliveira[19], M. Palatka[32], J. Pallotta[9], S. Panja[32], G. Parente[79], T. Paulsen[38], J. Pawlowsky[38], M. Pech[32], J. Pękala[70], R. Pelayo[65], L.A.S. Pereira[23], E.E. Pereira Martins[39,7], J. Perez Armand[20], C. Pérez Bertolli[7,41], L. Perrone[56,48], S. Petrera[45,46], C. Petrucci[57,46], T. Pierog[41], M. Pimenta[72], M. Platino[7], B. Pont[80], M. Pothast[81,80], M. Pourmohammad Shahvar[61,47], P. Privitera[89], M. Prouza[32], A. Puyleart[87], S. Querchfeld[38], J. Rautenberg[38], D. Ravignani[7], M. Reininghaus[39], J. Ridky[32], F. Riehn[79], M. Risse[44], V. Rizi[57,46], W. Rodrigues de Carvalho[80], E. Rodriguez[7,41], J. Rodriguez Rojo[11], M.J. Roncoroni[7], S. Rossoni[43], M. Roth[41], E. Roulet[1], A.C. Rovero[4], P. Ruehl[44], A. Saftoiu[73], M. Saharan[80], F. Salamida[57,46], H. Salazar[64], G. Salina[51], J.D. Sanabria Gomez[30], F. Sánchez[7], E.M. Santos[20], E. Santos[32],

F. Sarazin[85], R. Sarmento[72], R. Sato[11], P. Savina[91], C.M. Schäfer[41], V. Scherini[56,48], H. Schieler[41], M. Schimassek[34], M. Schimp[38], F. Schlüter[41], D. Schmidt[39], O. Scholten[15,i], H. Schoorlemmer[80,81], P. Schovánek[32], F.G. Schröder[90,41], J. Schulte[42], T. Schulz[41], S.J. Sciutto[3], M. Scornavacche[7,41], A. Segreto[53,47], S. Sehgal[38], S.U. Shivashankara[76], G. Sigl[43], G. Silli[7], O. Sima[73,b], F. Simon[40], R. Smau[73], R. Šmída[89], P. Sommers[k], J.F. Soriano[86], R. Squartini[10], M. Stadelmaier[32], D. Stanca[73], S. Stanič[76], J. Stasielak[70], P. Stassi[36], S. Strähnz[39], M. Straub[42], M. Suárez-Durán[14], T. Suomijärvi[37], A.D. Supanitsky[7], Z. Svozilikova[32], Z. Szadkowski[71], A. Tapia[29], C. Taricco[63,52], C. Timmermans[81,80], O. Tkachenko[41], P. Tobiska[32], C.J. Todero Peixoto[18], B. Tomé[72], Z. Torrès[36], A. Travaini[10], P. Travnicek[32], C. Trimarelli[57,46], M. Tueros[3], M. Unger[41], L. Vaclavek[33], M. Vacula[33], J.F. Valdés Galicia[68], L. Valore[60,50], E. Varela[64], A. Vásquez-Ramírez[30], D. Veberič[41], C. Ventura[27], I.D. Vergara Quispe[3], V. Verzi[51], J. Vicha[32], J. Vink[83], J. Vlastimil[32], S. Vorobiov[76], C. Watanabe[26], A.A. Watson[c], A. Weindl[41], L. Wiencke[85], H. Wilczyński[70], D. Wittkowski[38], B. Wundheiler[7], B. Yue[38], A. Yushkov[32], O. Zapparrata[14], E. Zas[79], D. Zavrtanik[76,77], M. Zavrtanik[77,76]

──────── • ────────
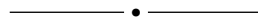
[1] Centro Atómico Bariloche and Instituto Balseiro (CNEA-UNCuyo-CONICET), San Carlos de Bariloche, Argentina

[2] Departamento de Física and Departamento de Ciencias de la Atmósfera y los Océanos, FCEyN, Universidad de Buenos Aires and CONICET, Buenos Aires, Argentina

[3] IFLP, Universidad Nacional de La Plata and CONICET, La Plata, Argentina

[4] Instituto de Astronomía y Física del Espacio (IAFE, CONICET-UBA), Buenos Aires, Argentina

[5] Instituto de Física de Rosario (IFIR) – CONICET/U.N.R. and Facultad de Ciencias Bioquímicas y Farmacéuticas U.N.R., Rosario, Argentina

[6] Instituto de Tecnologías en Detección y Astropartículas (CNEA, CONICET, UNSAM), and Universidad Tecnológica Nacional – Facultad Regional Mendoza (CONICET/CNEA), Mendoza, Argentina

[7] Instituto de Tecnologías en Detección y Astropartículas (CNEA, CONICET, UNSAM), Buenos Aires, Argentina

[8] International Center of Advanced Studies and Instituto de Ciencias Físicas, ECyT-UNSAM and CONICET, Campus Miguelete – San Martín, Buenos Aires, Argentina

[9] Laboratorio Atmósfera – Departamento de Investigaciones en Láseres y sus Aplicaciones – UNIDEF (CITEDEF-CONICET), Argentina

[10] Observatorio Pierre Auger, Malargüe, Argentina

[11] Observatorio Pierre Auger and Comisión Nacional de Energía Atómica, Malargüe, Argentina

[12] Universidad Tecnológica Nacional – Facultad Regional Buenos Aires, Buenos Aires, Argentina

[13] University of Adelaide, Adelaide, S.A., Australia

[14] Université Libre de Bruxelles (ULB), Brussels, Belgium

[15] Vrije Universiteit Brussels, Brussels, Belgium

[16] Centro Federal de Educação Tecnológica Celso Suckow da Fonseca, Petropolis, Brazil

[17] Instituto Federal de Educação, Ciência e Tecnologia do Rio de Janeiro (IFRJ), Brazil

[18] Universidade de São Paulo, Escola de Engenharia de Lorena, Lorena, SP, Brazil

[19] Universidade de São Paulo, Instituto de Física de São Carlos, São Carlos, SP, Brazil

[20] Universidade de São Paulo, Instituto de Física, São Paulo, SP, Brazil

[21] Universidade Estadual de Campinas, IFGW, Campinas, SP, Brazil

[22] Universidade Estadual de Feira de Santana, Feira de Santana, Brazil

[23] Universidade Federal de Campina Grande, Centro de Ciencias e Tecnologia, Campina Grande, Brazil

[24] Universidade Federal do ABC, Santo André, SP, Brazil

[25] Universidade Federal do Paraná, Setor Palotina, Palotina, Brazil

[26] Universidade Federal do Rio de Janeiro, Instituto de Física, Rio de Janeiro, RJ, Brazil

[27] Universidade Federal do Rio de Janeiro (UFRJ), Observatório do Valongo, Rio de Janeiro, RJ, Brazil

[28] Universidade Federal Fluminense, EEIMVR, Volta Redonda, RJ, Brazil

[29] Universidad de Medellín, Medellín, Colombia

[30] Universidad Industrial de Santander, Bucaramanga, Colombia

[31] Charles University, Faculty of Mathematics and Physics, Institute of Particle and Nuclear Physics, Prague, Czech Republic

[32] Institute of Physics of the Czech Academy of Sciences, Prague, Czech Republic

[33] Palacky University, Olomouc, Czech Republic

[34] CNRS/IN2P3, IJCLab, Université Paris-Saclay, Orsay, France

[35] Laboratoire de Physique Nucléaire et de Hautes Energies (LPNHE), Sorbonne Université, Université de Paris, CNRS-IN2P3, Paris, France

[36] Univ. Grenoble Alpes, CNRS, Grenoble Institute of Engineering Univ. Grenoble Alpes, LPSC-IN2P3, 38000 Grenoble, France

[37] Université Paris-Saclay, CNRS/IN2P3, IJCLab, Orsay, France

[38] Bergische Universität Wuppertal, Department of Physics, Wuppertal, Germany

[39] Karlsruhe Institute of Technology (KIT), Institute for Experimental Particle Physics, Karlsruhe, Germany

[40] Karlsruhe Institute of Technology (KIT), Institut für Prozessdatenverarbeitung und Elektronik, Karlsruhe, Germany

[41] Karlsruhe Institute of Technology (KIT), Institute for Astroparticle Physics, Karlsruhe, Germany

[42] RWTH Aachen University, III. Physikalisches Institut A, Aachen, Germany

[43] Universität Hamburg, II. Institut für Theoretische Physik, Hamburg, Germany

[44] Universität Siegen, Department Physik – Experimentelle Teilchenphysik, Siegen, Germany

[45] Gran Sasso Science Institute, L'Aquila, Italy

[46] INFN Laboratori Nazionali del Gran Sasso, Assergi (L'Aquila), Italy

[47] INFN, Sezione di Catania, Catania, Italy

[48] INFN, Sezione di Lecce, Lecce, Italy

[49] INFN, Sezione di Milano, Milano, Italy

[50] INFN, Sezione di Napoli, Napoli, Italy

[51] INFN, Sezione di Roma "Tor Vergata", Roma, Italy

[52] INFN, Sezione di Torino, Torino, Italy

[53] Istituto di Astrofisica Spaziale e Fisica Cosmica di Palermo (INAF), Palermo, Italy

[54] Osservatorio Astrofisico di Torino (INAF), Torino, Italy

[55] Politecnico di Milano, Dipartimento di Scienze e Tecnologie Aerospaziali , Milano, Italy

[56] Università del Salento, Dipartimento di Matematica e Fisica "E. De Giorgi", Lecce, Italy

[57] Università dell'Aquila, Dipartimento di Scienze Fisiche e Chimiche, L'Aquila, Italy

[58] Università di Catania, Dipartimento di Fisica e Astronomia "Ettore Majorana", Catania, Italy

[59] Università di Milano, Dipartimento di Fisica, Milano, Italy

[60] Università di Napoli "Federico II", Dipartimento di Fisica "Ettore Pancini", Napoli, Italy

[61] Università di Palermo, Dipartimento di Fisica e Chimica "E. Segrè", Palermo, Italy

[62] Università di Roma "Tor Vergata", Dipartimento di Fisica, Roma, Italy

[63] Università Torino, Dipartimento di Fisica, Torino, Italy

[64] Benemérita Universidad Autónoma de Puebla, Puebla, México

[65] Unidad Profesional Interdisciplinaria en Ingeniería y Tecnologías Avanzadas del Instituto Politécnico Nacional (UPIITA-IPN), México, D.F., México

[66] Universidad Autónoma de Chiapas, Tuxtla Gutiérrez, Chiapas, México

[67] Universidad Michoacana de San Nicolás de Hidalgo, Morelia, Michoacán, México

[68] Universidad Nacional Autónoma de México, México, D.F., México

[69] Universidad Nacional de San Agustin de Arequipa, Facultad de Ciencias Naturales y Formales, Arequipa, Peru

[70] Institute of Nuclear Physics PAN, Krakow, Poland

[71] University of Łódź, Faculty of High-Energy Astrophysics, Łódź, Poland

[72] Laboratório de Instrumentação e Física Experimental de Partículas – LIP and Instituto Superior Técnico – IST, Universidade de Lisboa – UL, Lisboa, Portugal

[73] "Horia Hulubei" National Institute for Physics and Nuclear Engineering, Bucharest-Magurele, Romania

[74] Institute of Space Science, Bucharest-Magurele, Romania

[75] University Politehnica of Bucharest, Bucharest, Romania

[76] Center for Astrophysics and Cosmology (CAC), University of Nova Gorica, Nova Gorica, Slovenia

[77] Experimental Particle Physics Department, J. Stefan Institute, Ljubljana, Slovenia

[78] Universidad de Granada and C.A.F.P.E., Granada, Spain

[79] Instituto Galego de Física de Altas Enerxías (IGFAE), Universidade de Santiago de Compostela, Santiago de Compostela, Spain

[80] IMAPP, Radboud University Nijmegen, Nijmegen, The Netherlands

[81] Nationaal Instituut voor Kernfysica en Hoge Energie Fysica (NIKHEF), Science Park, Amsterdam, The Netherlands

[82] Stichting Astronomisch Onderzoek in Nederland (ASTRON), Dwingeloo, The Netherlands

[83] Universiteit van Amsterdam, Faculty of Science, Amsterdam, The Netherlands

[84] Case Western Reserve University, Cleveland, OH, USA

[85] Colorado School of Mines, Golden, CO, USA

[86] Department of Physics and Astronomy, Lehman College, City University of New York, Bronx, NY, USA

[87] Michigan Technological University, Houghton, MI, USA

[88] New York University, New York, NY, USA

[89] University of Chicago, Enrico Fermi Institute, Chicago, IL, USA

[90] University of Delaware, Department of Physics and Astronomy, Bartol Research Institute, Newark, DE, USA

[91] University of Wisconsin-Madison, Department of Physics and WIPAC, Madison, WI, USA

——

[a] Louisiana State University, Baton Rouge, LA, USA

[b] also at University of Bucharest, Physics Department, Bucharest, Romania

[c] School of Physics and Astronomy, University of Leeds, Leeds, United Kingdom

[d] now at Agenzia Spaziale Italiana (ASI). Via del Politecnico 00133, Roma, Italy

[e] Fermi National Accelerator Laboratory, Fermilab, Batavia, IL, USA

[f] now at Graduate School of Science, Osaka Metropolitan University, Osaka, Japan

[g] now at ECAP, Erlangen, Germany

[h] Max-Planck-Institut für Radioastronomie, Bonn, Germany

[i] also at Kapteyn Institute, University of Groningen, Groningen, The Netherlands

[j] Colorado State University, Fort Collins, CO, USA

[k] Pennsylvania State University, University Park, PA, USA

Acknowledgments